Scientific Research Publishing

Materials Sciences and Applications, 2024, 15, 137-154
https://www.scirp.org/journal/msa
ISSN Online: 2153-1188
ISSN Print: 2153-117X

Effect of Exchange-Correlation Functional on the Structural, Mechanical, and Optoelectronic Properties of Orthorhombic $RbSrBr_3$ Perovskite

Fatema Najrin[1,2], Rabeya Bakar Sarna[1], Md. Alamin Sarker[1], Budrun Neher[1], Md. Mahbubur Rahman Bhuiyan[1*], Farid Ahmed[1]

[1]Department of Physics, Jahangirnagar University, Dhaka, Bangladesh
[2]Department of Electrical and Electronics Engineering, Green University of Bangladesh, Purbachal American City, Kanchan, Rupganj, Narayanganj-1461, Dhaka, Bangladesh
Email: *bhuiyanphysics@juniv.edu, rahmanmahbubur@ymail.com

How to cite this paper: Najrin, F., Sarna, R.B., Sarker, Md.A., Neher, B., Bhuiyan, Md.M.R. and Ahmed, F. (2024) Effect of Exchange-Correlation Functional on the Structural, Mechanical, and Optoelectronic Properties of Orthorhombic $RbSrBr_3$ Perovskite. *Materials Sciences and Applications*, **15**, 137-154.
https://doi.org/10.4236/msa.2024.156010

Received: May 13, 2024
Accepted: June 25, 2024
Published: June 28, 2024

Abstract

In the present study, the effect of the exchange-correlation functional on the structural, mechanical, and optoelectronic properties of orthorhombic $RbSrBr_3$ perovskite has been investigated using various functionals in Density Functional Theory (DFT) with the CASTEP code. The optimized lattice parameters are quite similar for all the functionals. The electronic properties have shown that $RbSrBr_3$ perovskite is a wide direct band gap compound with a band gap energy ranging from 4.296 eV to 4.494 eV for all the functionals. The mechanical parameters like elastic constants, Young's modulus, Shear modulus, Poisson's ratio, Pugh's ratio, and an anisotropic factor reveal that the $RbSrBr_3$ perovskite has ductile behavior and an anisotropic nature which signifies the mechanical stability of the compound. The Debye temperature might withstand lattice vibration heat. High absorption coefficient ($>10^4$ cm^{-1}), high optical conductivity, and very low reflectivity have been found in the $RbSrBr_3$ perovskite for all functions. The computed findings on the $RbSrBr_3$ perovskite suggested that the presented studied material is potentially applicable for photodetector and optoelectronic devices.

Keywords

Density Functional Theory, Mechanical Properties, Photodetector, Ductility, Anisotropic Factor

1. Introduction

Over the past decade, metal-halide perovskites (MHP) have generated interest for

their exceptional efficiency as both a photovoltaic material and a light-emitting device (LED) [1] [2] [3]. The perovskite ideal structure follows a specific pattern, with certain elements occupying specific positions. In this structure, a monovalent cation takes up the A position, a divalent cation (such as Sr^{2+} or Pb^{2+}) occupies the B position, and a monovalent halogen anion (such as Cl^{-}, Br^{-}, or I^{-}) fills the X position [4]. In 1978, hybrid organic-inorganic perovskites (HOIP) were reported [5] [6]. Hybrids use organic cations like methylammonium ($CH_3NH_3^+$), formamidinium ($HC(NH_2)_2^+$), or ethylammonium ($(C_2H_5)NH_3)^+$ in the A-site [7].

Perovskite possesses an extraordinary variety of physical and chemical properties, making it highly suitable for a diverse range of advanced applications. These include ferroelectricity, piezoelectricity, extremely high temperatures superconductivity, enormous magnetoresistance, charge ordering, thermoelectricity, as well as magneto-transport features [8] [9] [10] [11] [12]. Using the DFT FP-LAPW approach, Rai *et al.* utilized the GGA and mBJ-based functionals to calculate the electronic properties of the $RbMF_3$ (M = Be, Mg, Ca, Sr, Ba) compound. They stated that the mBJ approach was more accurate when compared to the GGA and LDA approaches [13]. In 2018, a study was conducted by AH Larbi *et al.* on the electronic and optical properties of orthorhombic $RbSrCl_3$ materials. They utilized the TB-mBJ functional, which yielded superior outcomes compared to the GGA-PBE approximation. The study found that the materials had a bandgap of 7.132 eV and 5.452 eV, respectively [14]. In 2020, a study by HM Ghaithan *et al.* examined the structural, electronic, and optical properties of $CsPbBr_3$ perovskite in cubic, tetragonal, and orthorhombic structures. The researchers used various exchange-correlation functionals (GGA-PBE, GGA-PBEsol, EV-GGA, mBJ-GGA, nmBJ-GGA, umBJ-GGA) to calculate these properties. They acquired the bands from mBJ-GGA and umBJ-GGA approaches, which demonstrated excellent agreement with experimental data [15]. Multiple researchers, such as K.E. Babu *et al.* [16] and Zhen-Li *et al.* [17], have explored the properties of cubic perovskites and their optical characteristics. In these investigations, the FP-LAPW method was employed. More specifically, the generalized gradient approximation (GGA) and LDA approaches were utilized.

A work that was very comparable to this one on orthorhombic $RbSrBr_3$ was not reported previously, as far as we are aware. We developed and explored orthorhombic $RbSrBr_3$ perovskite's geometrical, electrical, optical, and elastic properties using DFT simulations. For DFT calculations, we utilized four exchange-correlation functionals to analyze the different properties of $RbSrBr_3$.

2. Computational Details

The structural, mechanical, electronic, and optical properties of orthorhombic $RbSrBr_3$ perovskite have been studied employing DFT based on the Cambridge Serial Total Energy Package (CASTEP) code [18] [19] [20] [21] [22]. The Broyden-Fletcher-Goldfarb-Shanno (BFGS) algorithm is applied to geometrical optimization [23]. To get all the properties at the lowest ground state energy, the

structure has been optimized through generalized gradient approximation (GGA) of Perdew-Burke-Ernzerhof (PBE) [24] [25], revised PBE functional for solids (PBEsol) [26], Perdew-Wang (PW91) and local density approximation (LDA) functional Ceperley-Alder-Perdew-Zunger (CAPZ) using ultrasoft pseudopotential [27] with a plane-wave basis set with cut-off energy of 400 eV to get a comprehensive solution along with medium self-consistent field (SCF) tolerance in the program [28]. These functionals were chosen to study electronics and optical properties due to their broad theoretical foundations and good performance in similar experiments. Benchmarking standard GGA-PBE is accurate and efficient. The structure is improved by solid-state material optimization. Even if PBE replaced GGA-PW91, consistency is needed. LDA-CAPZ, a simplified local density approximation, shows advanced GGAs' effects. We receive stable, non-functional effects [29]. The structure has been optimized using $4 \times 1 \times 1$ Monkhorst-Pack [30] grid in the Brillouin zone of the unit cell. The lattice parameters and the atomic positions within the cell were optimized until the forces and total energy converged within 0.05 eV/Å, 2×10^{-5} eV/atom, and atomic displacement during geometry optimization was less than 0.002Å, respectively.

3. Result and Discussion

3.1. Structural Properties

In the present work, the orthorhombic structure of the $RbSrBr_3$ perovskite that is crystallized with cm cm space group (No. 63) has been optimized using GGA-PBE, GGA-PBEsol, GGA-PW91, and LDA-CAPZ functionals to find out the details of the structure and to judge the functional variation on the properties of the studied compound. The optimized geometrical structure of orthorhombic $RbSrBr_3$ perovskite obtained using various functionals has been depicted in **Figure 1**. The lattice constants (Å), cell volume ($Å^3$), ground state energy (eV), and bulk modulus have been presented in **Table 1**. The minimum values of lattice constants, volume, and ground state energy have been observed by utilizing the LDA-CAPZ functional. The GGA-PBE, GGA-PBEsol, GGA-PW91, and LDA-CAPZ functionals have been revealed in the orthorhombic phase of $RbSrBr_3$ perovskite. Compared to other methods, PBEsol-GGA lattice constants were comparable to experimental values.

3.2. Mechanical Properties

The elastic constants C_{ij} describes the crystal's mechanical and dynamical nature and shows how pressure deforms matter and subsequently returns it to its original shape [31]. Elastic constants impact qualities such as anisotropy, ductility, and hardness and are governed by stress-strain relationships. In an orthorhombic structure, the nine independent elastic constants C_{ij} (C_{11}, C_{12}, C_{13}, C_{22}, C_{23}, C_{33}, C_{44}, C_{55}, C_{66}) can satisfy the Born stability conditions, which are provided in **Table 2** and elastic stability criteria are $C_{11} > 0$, $C_{44} > 0$, $C_{55} > 0$, $C_{66} > 0$, $C_{11}C_{22} > C^2_{12}$, $C_{11}C_{22}C_{33} + 2C_{12}C_{13}C_{23} - C_{11}C^2_{23} - C_{22}C^2_{13} - C_{33}C^2_{12} > 0$ [32].

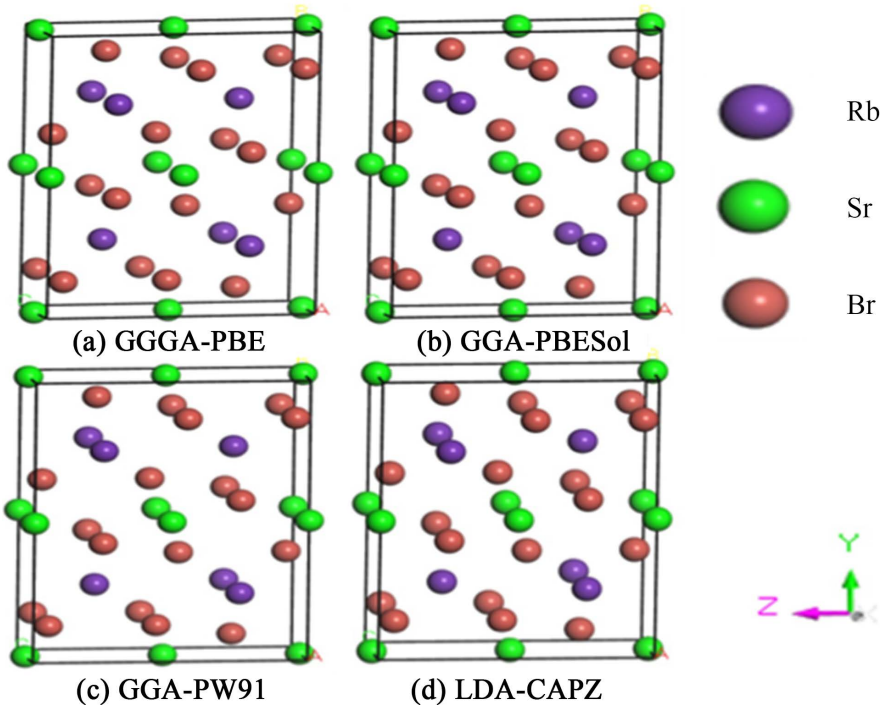

Figure 1. (a)-(d) The optimized geometrical structure of $RbSrBr_3$ perovskite using the GGA-PBE, GGA-PBEsol, GGA-PW91, and LDA-CAPZ approximation.

Table 1. Summarized lattice parameters, angle, volume, and ground state energy of $RbSrBr_3$ perovskite for different functional.

Functional	Lattice Parameters (Å)			Angle (Degree)			Volume (Å^3)	Ground state energy (eV)
	a	b	c	α	β	γ		
GGA-PBE	4.53	15.41	11.22	90	90	90	782.38	−10408.96
GGA-PBEsol	4.43	14.85	11.07	90	90	90	727.95	−10408.83
GGA-PW91	4.50	15.27	11.28	90	90	90	774.93	−10417.19
LDA-CAPZ	4.35	13.89	11.03	90	90	90	665.95	−10439.52

Table 2. Calculated elastic constants (GPa) of orthorhombic $RbSrBr_3$ structure for different functionals.

Functional	C_{11}	C_{12}	C_{13}	C_{22}	C_{23}	C_{33}	C_{44}	C_{55}	C_{66}
GGA-PBE	28.06	6.85	6.38	14.57	12.23	30.18	5.27	5.19	10.35
GGA-PBEsol	33.94	10.92	8.68	17.12	16.85	45.37	6.67	5.49	14.48
GGA-PW91	29.57	10.91	9.13	23.05	13.84	25.27	5.01	4.74	4.82
LDA-CAPZ	40.05	16.50	13.00	21.78	21.45	44.30	7.81	7.86	17.05

The elastic constants presented in **Table 2** indicate that orthorhombic $RbSrBr_3$ has m*et all* stability criteria, indicating mechanical stability for all the functionals. The elastic constants found for $RbSrBr_3$ are consistent with the theoretical results given in the literature [33]. The stiffness matrix [34] is positive definite using various functionals, as shown in the eigenvalues listed in **Table 3**. Fur-

thermore, the parameters, including Bulk modulus (B), shear modulus (G), Young's modulus (Y), Pugh's ratio (B/G), Poisson ratio (υ), and anisotropy (A) were measured. The nature of the bonding can be described by Cauchy pressure (C_p), according to Pettifor [35]. If C_P is positive, it means that the structure is flexible, and if it is negative, the combination will be brittle [36]. According to the condition above, the structure $RbSrBr_3$ is flexible using various functionals.

Table 3. Calculated eigenvalues of the stiffness matrix in GPa of $RbSrBr_3$ structure using various functionals

Functional	λ_1	λ_2	λ_3	λ_4	λ_5	λ_6
GGA-PBE	5.19	5.27	7.39	10.35	22.96	42.46
GGA-PBEsol	5.49	6.67	7.57	14.48	29.35	59.52
GGA-PW91	4.74	4.82	5.01	10.00	19.32	48.57
LDA-CAPZ	6.69	7.81	7.86	17.05	29.06	70.39

The shear modulus (G) shows how resistant the material is to changes in shape (bond angle) when pressure is applied from the outside. The bulk modulus (B) indicates the material's resistance to volumetric variations (bond length) [37]. 'E' represents Young's modulus, a method for determining the strength of a material. The value equals the stress-to-strain ratio [38]. Several methods, such as the Voigt, Reuss, and Hill techniques, can be used to derive estimates. Voigt suggested that the strain distribution in composite materials is homogenous [39]. The Reuss approximation is a commonly employed micromechanical model for studying composite materials. This model assumes that the composite phases experience equal stress, specifically normal stress [40]. The Hill convention is a numerical method that averages Reuss and Voigt values [41]. The parameters that determine the strength of the structure have been explained in **Table 4**.

$$B_H = \frac{B_V + B_R}{2} \tag{1}$$

$$G_H = \frac{G_V + G_R}{2} \tag{2}$$

These symbols B_H, B_V, B_R, G_H, G_V, and G_R correspond to the Hill bulk modulus, Voigt bulk modulus, Reuss bulk modulus, Hill shear modulus, Voigt shear modulus, and Reuss shear modulus.

Again, the following equation gives Young's modulus (E) and Poisson's ratio (υ) [42]

$$E = \frac{9B_H G_H}{3B_H + G_H} \tag{3}$$

$$\upsilon = \frac{3B_H - E}{6B_H} \tag{4}$$

The Poisson ratio is utilized in finite element simulations to design axially stressed components [43]. With the Hill G and B values, we can determine

Young's modulus and Poisson's ratio. For all functionals, the $RbSrBr_3$ perovskite has been predicted to be ductile, where $\upsilon \geq 1/3$ is comparable to the reference [44]. Pugh's ratio, Poisson's ratio, and Cauchy's pressure correlate with the material's stability and fragility. Pugh's ratio [45] suggested that the B/G ratio can indicate brittle or ductile material properties. The material is considered flexible when the ratio B to G is greater than 1.75; otherwise, it is classified as brittle. The orthorhombic of $RbSrBr_3$ structure has been showing flexible behavior for all the functionals.

Table 4. Calculated Bulk modulus B (GPa), Shear modulus G (GPa), Young modulus E (GPa), Pugh's ratio, Poisson's ratio υ, Compressibility 1/β (GPa^{-1}), Anisotropic factor A, Cauchy's pressure $C_p = C_{23} - C_{44}$ (GPa) of $RbSrBr_3$ using various functionals.

Functional	B (GPa)	G (GPa)	B/G	E (GPa)	υ	1/β (GPa^{-1})	A	C_p
GGA-PBE	13.05	6.67	1.96	17.10	0.28	0.08	1.19	6.96
GGA-PBEsol	17.30	8.11	2.13	21.05	0.30	0.06	1.95	10.18
GGA-PW91	16.18	5.64	2.87	15.15	0.34	0.06	0.39	8.83
LDA-CAPZ	21.94	8.80	2.49	23.28	0.32	0.05	2.05	13.64

Ranganathan and Ostoja-Starzewski established the universal anisotropic factor [46] to measure crystal anisotropy. The anisotropic factor is essential for understanding defect dynamics, structure stability, and compound elastic anisotropy [47].

$$A = \frac{G_V - G_R}{G_V + G_R} \tag{5}$$

The equation shows that the universal anisotropic A is greater than 1, which means that the crystalline structure of RbSrBr3 has elastic anisotropy [48].

Young's modulus, shear modulus, compressibility (the opposite of bulk modulus), and Poisson's ratio should be spherical for isotropic solids. If they don't stay in the shape of a sphere, it means that anisotropy is present. **Figure 2** revealed the directional dependency of Young's modulus, shear modulus, compressibility, and Poisson's ratio for the ELATE-generated $RbSrBr_3$ system [49].

The Debye temperature (θ_D), which correlates to the crystal's most extensive normal mode of vibration, is one of the most fundamental properties of solids. This parameter establishes a relationship between a solid's elastic and thermodynamic properties, containing phonons, thermal expansion, conductivity, specific heat, and lattice enthalpy. The average sound velocity, V_m and ρ, the mass density of the solid has to be used to calculate the Debye temperature (θ_D) The Debye temperature (θ_D) is given by [50].

$$\theta_D = \frac{h}{K_B} V_m \left[\frac{3n}{4\pi} \frac{\rho N_A}{M} \right]^{\frac{1}{3}} \tag{6}$$

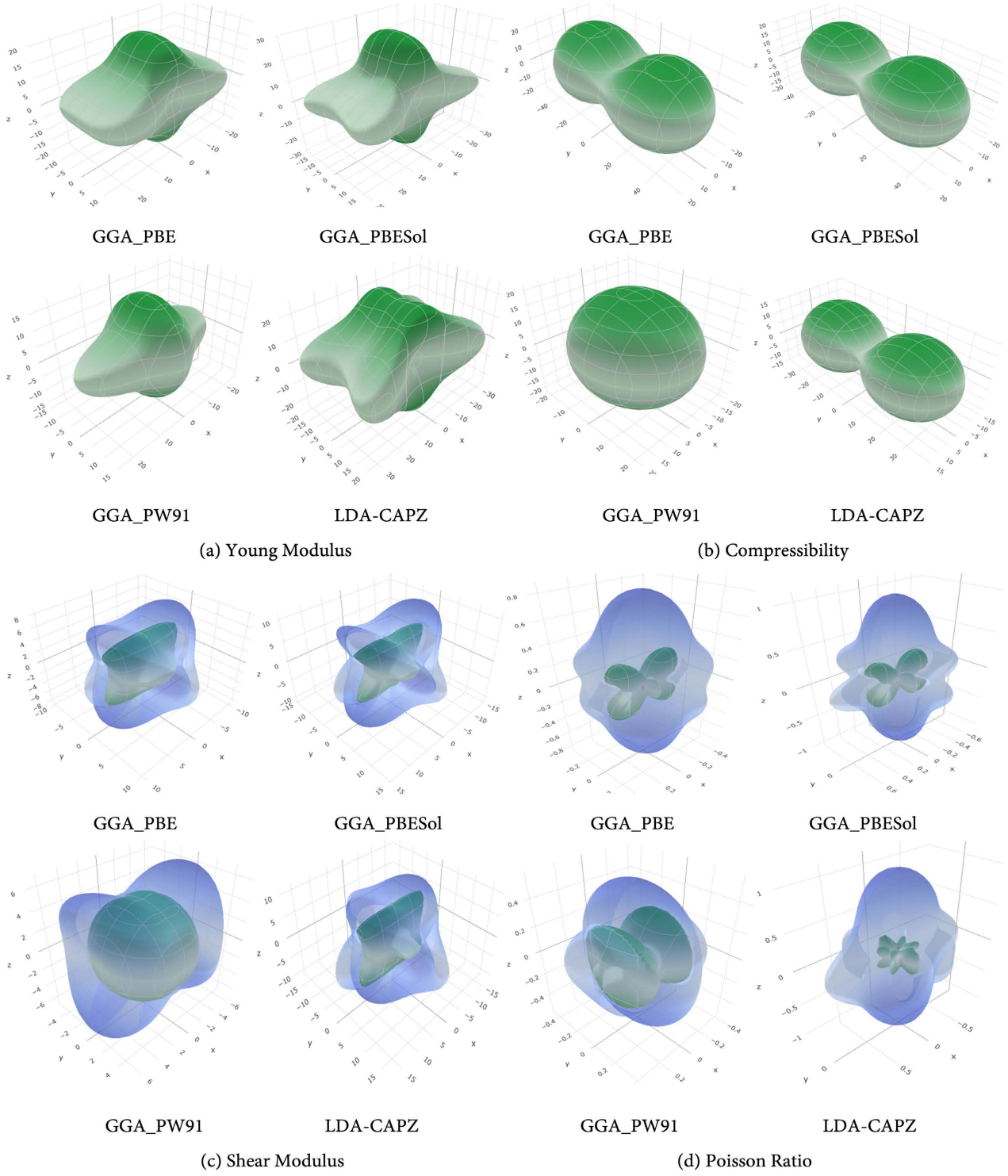

Figure 2. 3D directional dependences of $RbSrBr_3$'s (a) Young modulus, (b) compressibility, (c) shear modulus, and (d) Poisson's ratio using various functionals.

In Equation (6), h represents Planck's constant, k_B represents Boltzmann's constant, N_A represents Avogadro's number, ρ represents mass density, M represents molecular weight, and n represents the number of atoms in the cell. The LDA-CAPZ functional has been calculated to be the highest, and the GGA-PW91

functional has shown the lowest Debye Temperature, (θ_D) for $RbSrBr_3$, which is listed in Table 5. The cut-off debye temperature determines the lattice stability [51]. At temperatures below the Debye temperature, the atomic motion within the crystal lattice is negligible, enabling the free movement of electrons through the lattice planes with minimal dispersion due to the low electron-phonon coupling [52]. This solid becomes a weak heat conductor when the scattering level increases above the Debye temperature.

Table 5. Calculated values of transverse sound wave velocity (V_T) and longitudinal sound wave velocity (V_L), average sound velocity (V_m), melting temperature (T_m), and Debye temperature (θ_D) of $RbSrBr_3$ using various functionals.

Functional	V_T (m/s)	V_L (m/s)	Average sound velocity, V_m (m/s)	Melting Temperature, T_m (K)	Debye Temperature, θ_D (K)
GGA-PBE	2751.33	4991.11	3066.16	483.45	131.90
GGA-PBEsol	2925.28	5446.45	3359.95	523.88	142.37
GGA-PW91	2518.62	5166.56	2830.79	480.62	123.67
LDA-CAPZ	2916.43	5704.42	3267.57	540.60	147.72

From the obtained bulk modulus (B) and shear modulus (G), the calculations of the average sound velocity (V_m), transverse sound velocity (V_T), and longitudinal sound wave velocity (V_L) are derived using Navier's equation [53] which is given below:

$$V_m = \left[\frac{1}{3}\left(\frac{1}{V_L^3} + \frac{2}{V_T^3}\right)\right]^{-\frac{1}{3}} \tag{7}$$

$$V_T = \sqrt{\frac{G}{\rho}} \tag{8}$$

$$V_L = \sqrt{\frac{3B + 4G}{3\rho}} \tag{9}$$

Table 5 shows that the speed of the longitudinal wave is twice that of the transverse wave, which is comparable to the literature [36].

Fine *et al.* put together an empirical formula to obtain the melting temperature T_m of this structure via elastic constants [54]

$$T_m = 354 + 1.5\left(2C_{11} + C_{33}\right) \tag{10}$$

The melting temperature of crystalline materials indicates cohesive energy, atomic bond strength, and lattice anharmonicity. This material's melting temperature was found to be low, which means it is soft. The observed T_m values for all the functionals are lower than those of $PbMO_3$ (M = Sb, Bi) [55].

3.3. Electronic Structure

3.3.1. Band Structure

The electronic band structure of $RbSrBr_3$ perovskite has been calculated using

various functionals (GGA-PBE, GGA-PBEsol, GGA-PW91, LDA-CAPZ) through the symmetry points of the Brillouin zone (G→Z→T→Y→S→X→U→R) where the valence band maximum (VBM) was fixed at 0 eV. The band structure of $RbSrBr_3$ perovskite for all the functionals has been presented in **Figure 3**. The values of bandgap for four different functions lie between 4.293 eV to 4.494 eV. The lowest band gap has been found using GGA-PBE functional, whereas the highest band gap has been obtained using GGA-PBEsol functional. The obtained values of band gap of the present studied perovskite signify that they are insulating-like. The size, form, symmetry, and geometry of the Brillouin zone have been modified by the band structure [56]. Direct band gap nature has been found in $RbSrBr_3$ structure for all functions because the valence band maximum (VBM) and conduction band minimum (CBM) have been found at the "G" of the K-point.

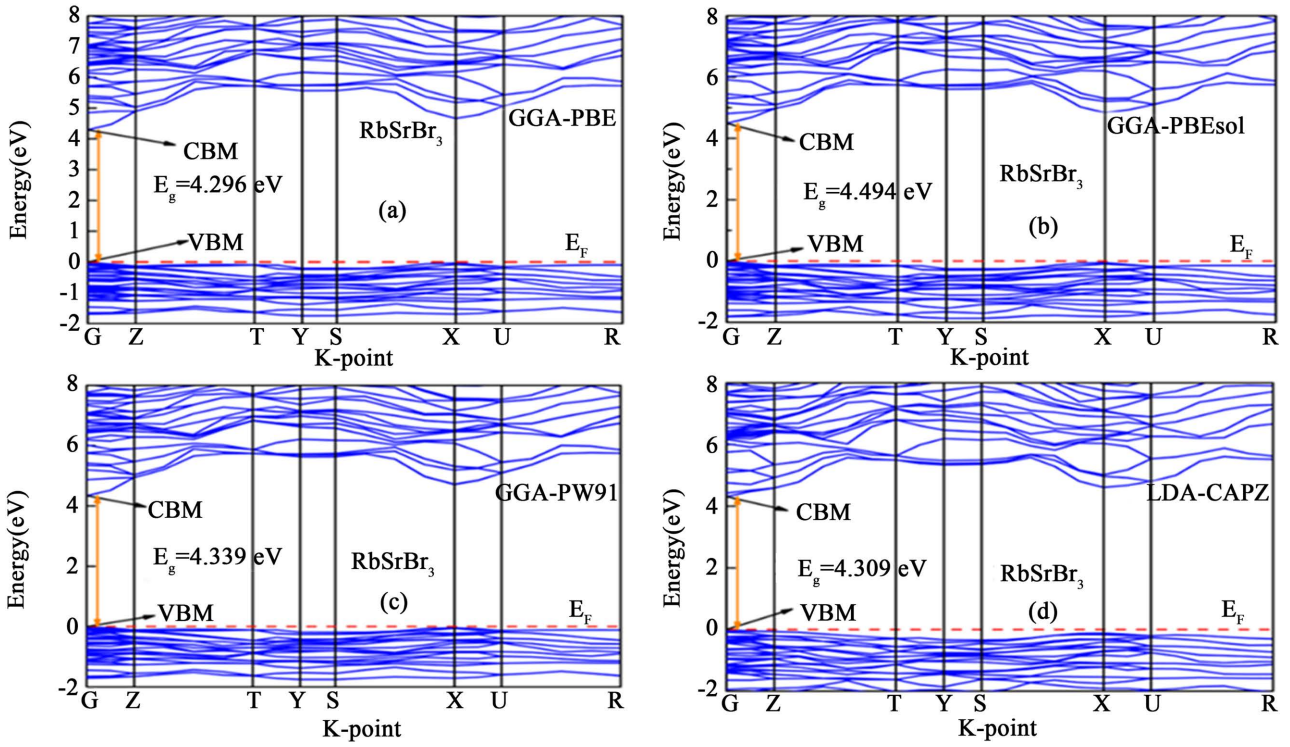

Figure 3. Calculated electronic band structure of $RbSrBr_3$ found using (a) GGA-PBE, (b) GGA-PBEsol, (c) GGA-PW91, (d) LDA-CAPZ functionals.

3.3.2. Density of State

The total density of state (TDOS) and partial density of state (PDOS) of orthorhombic $RbSrBr_3$ structure calculated using various functionals have been presented in **Figure 4(a)-(d)**. **Figure 4(e)** represents the compared total density of states (TDOS) of $RbSrBr_3$ structure among four different functions. The atomic bonding in the $RbSrBr_3$ compound has been investigated through PDOS. The valence band maximum for all functionals has been formed from the p orbital of Br, with a small contribution from the d orbital of Sr. On the other hand, the

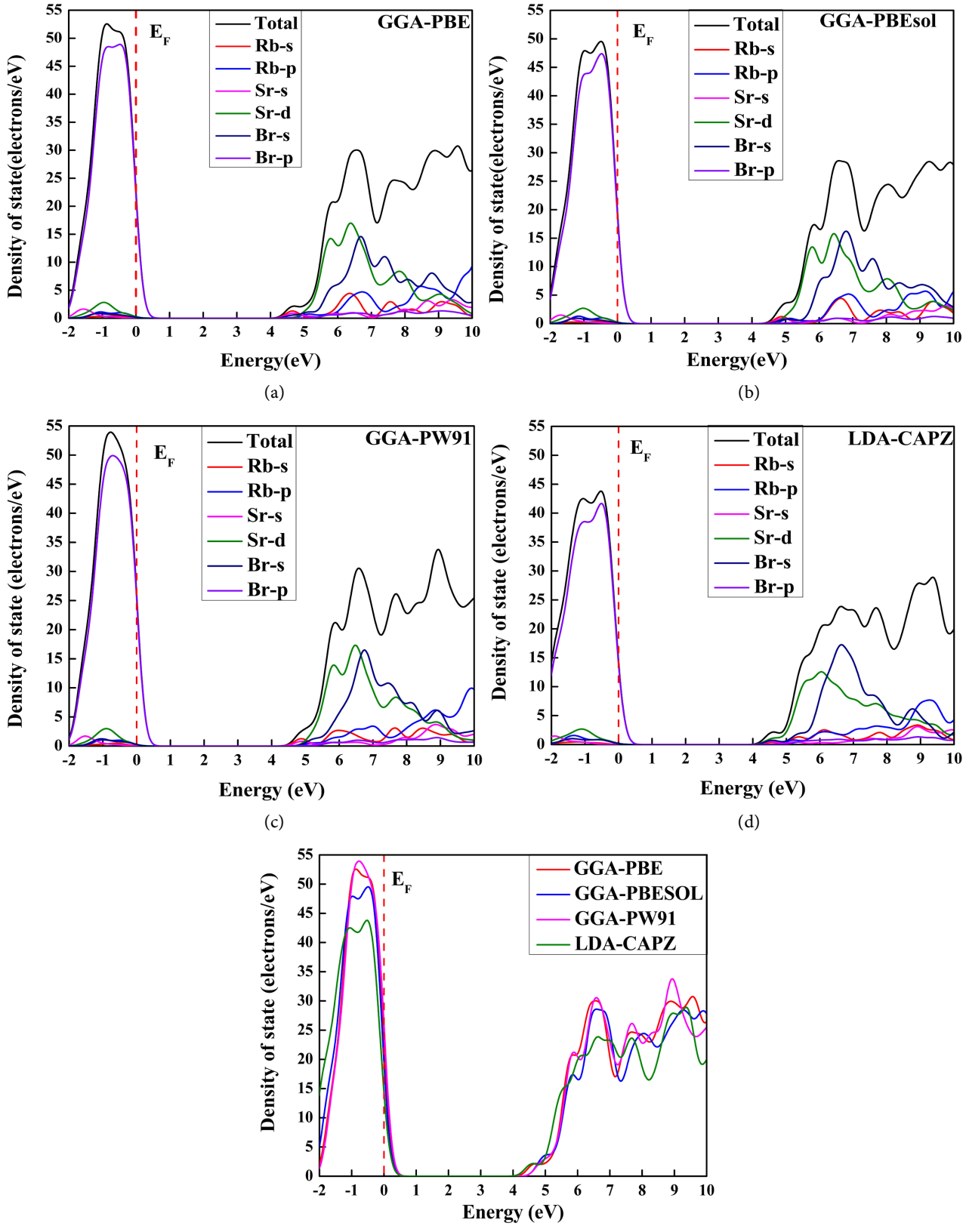

Figure 4. Calculated Partial Density of State (PDOS) of $RbSrBr_3$ utilizing (a) GGA-PBE, (b) GGA-PBEsol, (c) GGA-PW91, (d) LDA-CAPZ functionals, and (e) Compared Total Density of State (TDOS) of $RbSrBr_3$ structure for four different functions.

conduction band minimum has been derived from the d orbital of Sr with a minor contribution from the s orbital of Sr using various functionals [15]. The total density of states (TDOS) plotted in **Figure 4** revealed that the halogen atom (Br) at the Fermi level edges contributes significantly to DOS in VB, resulting in flat bands at the band edges [57].

3.4. Optical Properties

The optical characteristics of a material have an inherent connection to its ground-state electrical configuration. Different optical properties of the orthorhombic $RbSrBr_3$ structure with the variation of energy (eV) for different functions have been presented in **Figure 5** and **Figure 6**.

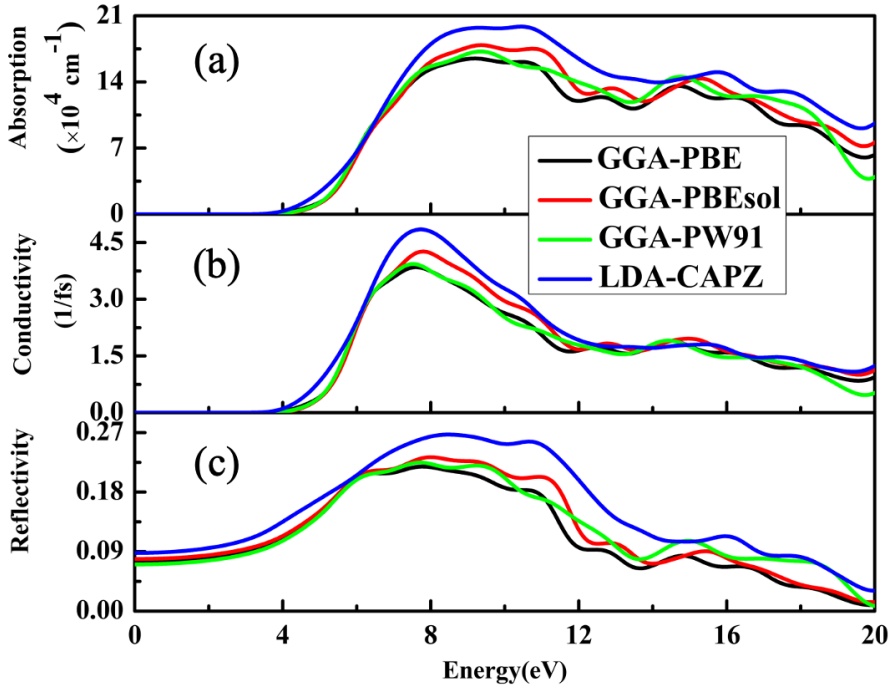

Figure 5. Variations of absorption coefficient, optical conductivity, and reflectivity for change in energy (eV) for $RbSrBr_3$ structure using different functionals.

The absorption coefficient is a measure of the photon absorption ability of materials [58]. The absorption coefficient of orthorhombic $RbSrBr_3$ perovskite has been presented in **Figure 5(a)**. The major absorption peaks have been obtained at 9.21 eV, 9.21 eV, 9.30 eV, and 8.88 eV for GGA-PBE, GGA-PBEsol, GGA-PW91, and LDA-CAPZ, respectively. The higher value of absorption peak ($>10^4$ cm^{-1}) has been found almost at the same energy for all functions and all major peaks lie in the UV region.

The optical conductivity spectrum represents the quantity of free charge carriers generated through bond breakage during electron-photon interaction [59]. The optical conductivity is shown in **Figure 5(b)**. The highest peaks have been obtained at 7.52 eV, 7.73 eV, 7.44 eV, and 7.69 eV for GGA-PBE, GGA-PBEsol, GGA-PW91, and LDA-CAPZ, respectively. In this structure, zero optical con-

ductivity (OC) and higher optical conductivity (OC) have been found in the UV, and Visible regions for all the functions.

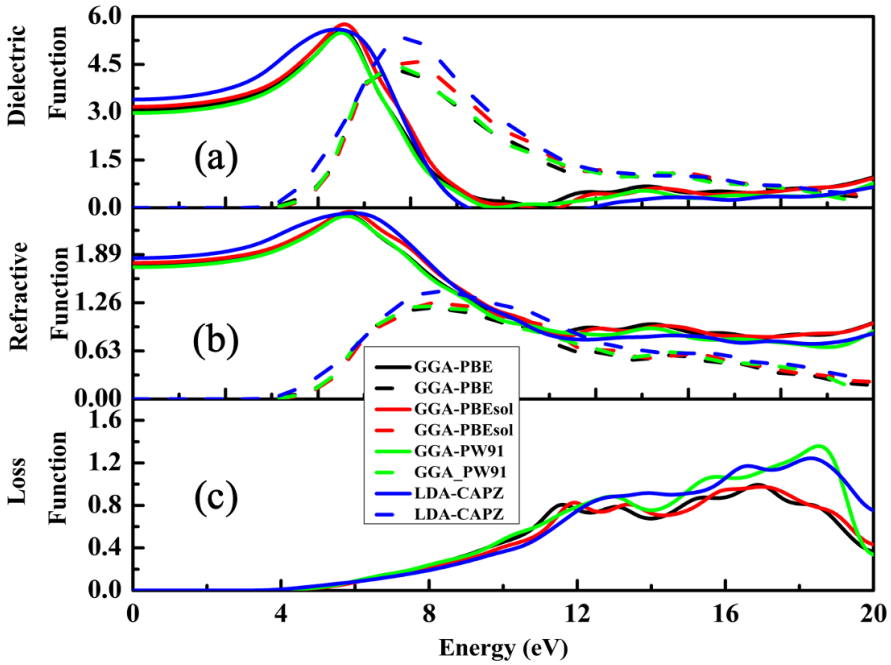

Figure 6. The variation of (a) dielectric function, (b) refractive index, and (c) loss function concerning change in energy (eV) for $RbSrBr_3$ for different functionals.

Reflectivity measures the fraction of energy that is reflected from the crystal structure [60]. It has been varied from zero to unit. The absorption of light and reflectivity are closely related to each other. The variation of reflectivity with the change of energy in the $RbSrBr_3$ structure for all functions is presented in **Figure 5(c)**. The lowest value of reflectivity has been found in the visible and IR regions for all the functions.

The dielectric function can be expressed as [61]

$$\varepsilon(\omega) = \varepsilon_1(\omega) + i\varepsilon_2(\omega) \tag{11}$$

Here, $\varepsilon_1(\omega)$ represents a real part of the dielectric function. The higher value of the real part of the dielectric function indicates a stronger ability of the material to polarize in response to the electric field. The imaginary part $\varepsilon_2(\omega)$ signifies the molecular polarization loss due to fluctuations in the external electric field [62]. The dielectric function of orthorhombic $RbSrBr_3$ perovskite has been illustrated in **Figure 6(a)**. The imaginary part and the real part are connected through the Kramers-Kronig relationships [63]. The absorption coefficient has been found in the imaginary part of the dielectric function. The threshold energy for the imaginary dielectric function has been found at 3.90 eV for all the functionals that were correlated with the energy band gap and worked for the UV-region. The principal peak has been located at 6.87 eV, 7.52 eV, 6.87 eV and 6.24 eV for GGA-PBE, PBEsol, PW91 and LDA-CAPZ functionals, respectively. The static dielectric function has been obtained at 5.67 eV for all functionals.

The Penn relation ($\varepsilon_1(0) \approx 1 + (\hbar\omega/E_g)^2$) represents that the static dielectric function is inversely proportional to the energy band gap. The dielectric function becomes negative with the increment of energy, indicating that the medium reflects electromagnetic waves, exhibiting its metallic properties.

The complex refractive function has been calculated by the relation:

$$N = n(\omega) + ik(\omega) \tag{12}$$

where $n(\omega)$ and $k(\omega)$ are the refractive index and the extinction index, respectively, which could be found from a real and imaginary portion of the dielectric function employing the previously mentioned relation [64]. The refractive function versus energy curve has been found in **Figure 6(b)**. The value of the refractive index of $RbSrBr_3$ structure was 1.78, 1.79, 1.70, and 1.87 for GGA-PBE, PBEsol, PW91, and LDA-CAPZ functions, respectively. The refractive index peak is found in the UV region for all the functions, and it decreases with the increase of energy. Extinction coefficient $k(\omega)$ signifies the light absorption ability of the compound at a certain range. The profiles of $k(\omega)$ and $\varepsilon_2(\omega)$ were closely connected in their respective functionals. The loss function $L(\omega)$ has been displaced in **Figure 6(c)**. The function $L(\omega)$ is essential for representing the energy that fast electrons lose as they move through a solid [65]. The peaks observed in the $L(\omega)$ spectra have been suggestive of the properties related to the plasma resonance. The resonant energy loss was obtained at 12.04 eV.

4. Conclusion

In summary, the structural, mechanical, and optoelectronic properties of inorganic orthorhombic $RbSrBr_3$ perovskite have been studied employing GGA-PBE, GGA-PBEsol, GGA-PW91, and LDA-CAPZ functions using density functional theory (DFT). The optimized lattice parameters of the $RbSrBr_3$ perovskite fulfilled the criteria of orthorhombic crystal structure using all the functions. The obtained electronic band gaps of orthorhombic $RbSrBr_3$ perovskite are 4.296 eV, 4.494 eV, 4.339 eV, and 4.309 eV using GGA-PBE, GGA-PBEsol, GGA-PW91, and LDA-CAPZ functionals, respectively. Moreover, every band gap has been found direct band gap in nature. The occupied valence band (VB) and unoccupied conduction band (CB) have occurred at the 'G' point for every function. The GGA-PBEsol functional has the highest band gap, and the GGA-PBE functional has the lowest band gap. The total and partial density of states were discussed in detail, which is comparable to the reference. The orthorhombic $RbSrBr_3$ perovskite has been found mechanically stable at all functionals. According to Pugh's ratio and Poisson's ratio, the structure has shown ductile behavior. The value of the anisotropic factor was greater than 1, and the 3D structure of Young's modulus, Shear modulus, Compressibility, and Poisson ratio are an anisotropic nature. The higher absorption > 10^4 cm^{-1}) makes the studied structure as potential candidate for the absorber layer. Refractive index and reflectivity measurement indicate significant photon energy loss in the $RbSrBr_3$ structure. The present study reflects that the $RbSrBr_3$ structure is a promising

candidate for scintillator applications and an anti-reflection coating material because of having a wide band gap, optical isotropy, and structural anisotropy nature in the structure.

Data Availability Statement

The data that support the findings of this study are available from the corresponding author upon reasonable request.

Conflicts of Interest

No potential conflict of interest was reported by the authors.

References

[1] De Angelis, F. (2018) Perovskite Solar Cells in the Public Domain as the Community Gears up for Technical Advances. *ACS Energy Letters*, **3**, 890-891. https://doi.org/10.1021/acsenergylett.8b00403

[2] Stranks, S.D. and Snaith, H.J. (2015) Metal-Halide Perovskites for Photovoltaic and Light-Emitting Devices. *Nature Nanotechnology*, **10**, 391-402. https://doi.org/10.1038/nnano.2015.90

[3] Liang, J., Liu, J. and Jin, Z. (2017) All-Inorganic Halide Perovskites for Optoelectronics: Progress and Prospects. *Solar RRL*, **1**, Article 1700086. https://doi.org/10.1002/solr.201700086

[4] Ornelas-Cruz, I., Trejo, A., Oviedo-Roa, R., Salazar, F., Carvajal, E., Miranda, A., *et al.* (2020) DFT-Based Study of the Bulk Tin Mixed-Halide $CsSnI_{3-x}$ Br_x Perovskite. *Computational Materials Science*, **178**, Article 109619. https://doi.org/10.1016/j.commatsci.2020.109619

[5] Stoumpos, C.C., Malliakas, C.D. and Kanatzidis, M.G. (2013) Semiconducting Tin and Lead Iodide Perovskites with Organic Cations: Phase Transitions, High Mobilities, and Near-Infrared Photoluminescent Properties. *Inorganic Chemistry*, **52**, 9019-9038. https://doi.org/10.1021/ic401215x

[6] Weber, D. (1978) $CH_3NH_3PbX_3$, ein Pb(II)-System Mit Kubischer Perowskitstruktur/$CH_3NH_3PbX_3$, a Pb(II)-System with Cubic Perovskite Structure. *Zeitschrift für Naturforschung B*, **33**, 1443-1445. https://doi.org/10.1515/znb-1978-1214

[7] Gholipour, S., Ali, A.M., Correa-Baena, J., Turren-Cruz, S., Tajabadi, F., Tress, W., *et al.* (2017) Globularity-Selected Large Molecules for a New Generation of Multication Perovskites. *Advanced Materials*, **29**, Article 1702005. https://doi.org/10.1002/adma.201702005

[8] Ippili, S., Jella, V., Kim, J., Hong, S. and Yoon, S. (2018) Enhanced Piezoelectric Output Performance via Control of Dielectrics in Fe^{2+}-Incorporated MAPBI3 Perovskite Thin Films: Flexible Piezoelectric Generators. *Nano Energy*, **49**, 247-256. https://doi.org/10.1016/j.nanoen.2018.04.031

[9] Fan, Z., Xiao, J., Sun, K., Chen, L., Hu, Y., Ouyang, J., *et al.* (2015) Ferroelectricity of $CH_3NH_3PBI_3$ Perovskite. *The Journal of Physical Chemistry Letters*, **6**, 1155-1161. https://doi.org/10.1021/acs.jpclett.5b00389

[10] Röhm, H., Leonhard, T., Schulz, A.D., Wagner, S., Hoffmann, M.J. and Colsmann, A. (2019) Ferroelectric Properties of Perovskite Thin Films and Their Implications for Solar Energy Conversion. *Advanced Materials*, **31**, Article 1806661. https://doi.org/10.1002/adma.201806661

[11] Kan, D. and Shimakawa, Y. (2019) Strain Effect on Thermoelectric Properties of $SrRuO_3$ Epitaxial Thin Films. *Applied Physics Letters*, **115**, Article 022403. https://doi.org/10.1063/1.5097927

[12] Kobayashi, K., Kan, D., Matsumoto, S., Mizumaki, M. and Shimakawa, Y. (2019) Orbital Magnetic Moments in Strained $SrRuO_3$ Thin Films. *Journal of the Physical Society of Japan*, **88**, Article 084708. https://doi.org/10.7566/jpsj.88.084708

[13] Sandeep, Rai, D.P., Shankar, A., Ghimire, M.P., Khenata, R., Bin Omran, S., *et al.* (2017) Investigation of the Structural, Electronic and Optical Properties of the Cubic $RbMF_3$ Perovskites (M=Be, Mg, Ca, Sr and Ba) Using Modified Becke-Johnson Exchange Potential. *Materials Chemistry and Physics*, **192**, 282-290. https://doi.org/10.1016/j.matchemphys.2017.02.005

[14] Hadj Larbi, A., Hiadsi, S., Hadjab, M. and Saeed, M.A. (2018) Optical Study of Cubic, and Orthorhombic Structures of $XCaCl_3$ (X=K, Rb) Compounds: Comparative Ab Initio Calculations. *Optik*, **166**, 169-176. https://doi.org/10.1016/j.ijleo.2018.03.128

[15] Ghaithan, H.M., Alahmed, Z.A., Qaid, S.M.H., Hezam, M. and Aldwayyan, A.S. (2020) Density Functional Study of Cubic, Tetragonal, and Orthorhombic $CsPbBr_3$ Perovskite. *ACS Omega*, **5**, 7468-7480. https://doi.org/10.1021/acsomega.0c00197

[16] Babu, K.E., Veeraiah, A., Swamy, D.T. and Veeraiah, V. (2012) First-Principles Study of Electronic Structure and Optical Properties of Cubic Perovskite $CsCaF_3$. *Chinese Physics Letters*, **29**, Article 117102. https://doi.org/10.1088/0256-307x/29/11/117102

[17] Li, Z., An, X., Cheng, X., Wang, X., Zhang, H., Peng, L., *et al.* (2014) First-Principles Study of the Electronic Structure and Optical Properties of Cubic Perovskite $NaMgF_3$. *Chinese Physics B*, **23**, Article 037104. https://doi.org/10.1088/1674-1056/23/3/037104

[18] Segall, M.D., Lindan, P.J.D., Probert, M.J., Pickard, C.J., Hasnip, P.J., Clark, S.J., *et al.* (2002) First-Principles Simulation: Ideas, Illustrations and the CASTEP Code. *Journal of Physics: Condensed Matter*, **14**, 2717-2744. https://doi.org/10.1088/0953-8984/14/11/301

[19] Clark, S.J., Segall, M.D., Pickard, C.J., Hasnip, P.J., Probert, M.I.J., Refson, K., *et al.* (2005) First Principles Methods Using CASTEP. *Zeitschrift für Kristallographie-Crystalline Materials*, **220**, 567-570. https://doi.org/10.1524/zkri.220.5.567.65075

[20] Maeda, T., Kawabata, A. and Wada, T. (2015) First-Principles Study on Alkali-Metal Effect of Li, Na, and K in Cu_2ZnSnS_4 and $Cu_2ZnSnSe_4$. Physica Status Solidi C, **12**, 631-637. https://doi.org/10.1002/pssc.201400345

[21] Kohn, W. and Vashishta, P. (1983) General Density Functional Theory. In: Lundqvist, S. and March, N.H., Eds., *Theory of the Inhomogeneous Electron Gas*, Springer, 79-147. https://doi.org/10.1007/978-1-4899-0415-7_2

[22] Kohn, W. and Sham, L.J. (1965) Self-Consistent Equations Including Exchange and Correlation Effects. *Physical Review*, **140**, A1133-A1138. https://doi.org/10.1103/physrev.140.a1133

[23] Zhao, W. (2021) A Broyden-Fletcher-Goldfarb-Shanno Algorithm for Reliability-Based Design Optimization. *Applied Mathematical Modelling*, **92**, 447-465. https://doi.org/10.1016/j.apm.2020.11.012

[24] Perdew, J.P., Burke, K. and Ernzerhof, M. (1996) Generalized Gradient Approximation Made Simple. *Physical Review Letters*, **77**, 3865-3868.

https://doi.org/10.1103/physrevlett.77.3865

[25] Wu, Z. and Cohen, R.E. (2006) More Accurate Generalized Gradient Approximation for Solids. *Physical Review B*, **73**, Article 235116. https://doi.org/10.1103/physrevb.73.235116

[26] Pedroza, L.S., da Silva, A.J.R. and Capelle, K. (2009) Gradient-Dependent Density Functionals of the Perdew-Burke-Ernzerhof Type for Atoms, Molecules, and Solids. *Physical Review B*, **79**, Article 201106. https://doi.org/10.1103/physrevb.79.201106

[27] Smith, J.M., Jones, S.P. and White, L.D. (1977) Rapid Communication. *Gastroenterology*, **72**, 193. https://doi.org/10.1016/s0016-5085(77)80340-5

[28] McWeeny, R. (1968) Multi-Configuration SCF Calculations. *Symposia of the Faraday Society*, **2**, 7-14. https://doi.org/10.1039/sf9680200007

[29] He, L., Liu, F., Hautier, G., Oliveira, M.J.T., Marques, M.A.L., Vila, F.D., *et al.* (2014) Accuracy of Generalized Gradient Approximation Functionals for Density-Functional Perturbation Theory Calculations. *Physical Review B*, **89**, Article 064305. https://doi.org/10.1103/physrevb.89.064305

[30] Monkhorst, H.J. and Pack, J.D. (1976) Special Points for Brillouin-Zone Integrations. *Physical Review B*, **13**, 5188-5192. https://doi.org/10.1103/physrevb.13.5188

[31] Arar, R., Ouahrani, T., Varshney, D., Khenata, R., Murtaza, G., Rached, D., *et al.* (2015) Structural, Mechanical and Electronic Properties of Sodium Based Fluoroperovskites $NaXF_3$ (X=Mg, Zn) from First-Principle Calculations. *Materials Science in Semiconductor Processing*, **33**, 127-135. https://doi.org/10.1016/j.mssp.2015.01.040

[32] Born, M. (1940) On the Stability of Crystal Lattices. I. *Mathematical Proceedings of the Cambridge Philosophical Society*, **36**, 160-172. https://doi.org/10.1017/s0305004100017138

[33] Roknuzzaman, M., Ostrikov, K., Wang, H., Du, A. and Tesfamichael, T. (2017) Towards Lead-Free Perovskite Photovoltaics and Optoelectronics by *ab-initio* Simulations. *Scientific Reports*, **7**, Article No. 14025. https://doi.org/10.1038/s41598-017-13172-y

[34] Angeles, J., (2010), On the Nature of the Cartesian Stiffness Matrix, Ingeniería Mecánica, *Tecnologíay Desarrollo*, **3**, 163-170.

[35] Pettifor, D.G. (1992) Theoretical Predictions of Structure and Related Properties of Intermetallics. *Materials Science and Technology*, **8**, 345-349. https://doi.org/10.1179/mst.1992.8.4.345

[36] Mondal, P., Hossain, K., Khanom, M.S., Hossain, M.K. and Ahmed, F. (2023) First-Principles Calculations to Investigate Structural, Elastic, Thermodynamic, Electronic, and Optical Properties of $AgXCL_3$ (X=Fe, Co & Mn). *Computational Condensed Matter*, **37**, e00860. https://doi.org/10.1016/j.cocom.2023.e00860

[37] Duan, Y., Hu, W., Sun, Y. and Peng, M. (2014) Structural and Anisotropic Elastic Properties of Zintl M_2Pb (M=Ca, Sr and Ba) Compounds as a Function of Pressure. *Journal of Alloys and Compounds*, **614**, 334-344. https://doi.org/10.1016/j.jallcom.2014.06.100

[38] Bootchanont, A., Phacheerak, K., Fongkaew, I., Limpijumnong, S. and Sailuam, W. (2021) The Pressure Effect on the Structural, Elastic, and Mechanical Properties of Orthorhombic $MgSiN_2$ from First-Principles Calculations. *Solid State Communications*, **336**, Article 114318. https://doi.org/10.1016/j.ssc.2021.114318

[39] Voigt, W. (1928) Lehrbuch der kristallphysik. Teubner Verlag.

[40] Reuss, A. (1929) Berechnung der Fließgrenze von Mischkristallen auf Grund der

Plastizitätsbedingung für Einkristalle. *ZAMM-Journal of Applied Mathematics and Mechanics/Zeitschrift für Angewandte Mathematik und Mechanik*, **9**, 49-58. https://doi.org/10.1002/zamm.19290090104

[41] Hill, R. (1952) The Elastic Behaviour of a Crystalline Aggregate. *Proceedings of the Physical Society. Section A*, **65**, 349-354. https://doi.org/10.1088/0370-1298/65/5/307

[42] Mehl, M.J., Klein, B.M. and Papaconstantopoulos, D.A. (1994) First-Principles Calculation of Elastic Properties of Metals Vol.1. In: Westbrook, J.H. and Fleischer, R.L., Eds., *Intermetallic Compounds-Principles and Practice*, John Wiley & Sons, 195-210.

[43] Fried, I. (1973) Influence of Poisson's Ratio on the Condition of the Finite Element Stiffness Matrix. *International Journal of Solids and Structures*, **9**, 323-329. https://doi.org/10.1016/0020-7683(73)90083-8

[44] Frantsevich, I.N., Voronov, F.F. and Bakuta, S.A. (1982) Elastic Constants and Elastic Moduli of Metals and Nonmetals (In Russian). Izdatel'stvo Naukova Dumka, Kiev, 288.

[45] Pugh, S.F. (1954) XCII. Relations between the Elastic Moduli and the Plastic Properties of Polycrystalline Pure Metals. *The London, Edinburgh, and Dublin Philosophical Magazine and Journal of Science*, **45**, 823-843. https://doi.org/10.1080/14786440808520496

[46] Ranganathan, S.I. and Ostoja-Starzewski, M. (2008) Universal Elastic Anisotropy Index. *Physical Review Letters*, **101**, Article 055504. https://doi.org/10.1103/physrevlett.101.055504

[47] Sundareswari, M., Ramasubramanian, S. and Rajagopalan, M. (2010) Elastic and Thermodynamical Properties of A15 Nb_3X (X=Al, Ga, In, Sn and Sb) Compounds—First Principles DFT Study. *Solid State Communications*, **150**, 2057-2060. https://doi.org/10.1016/j.ssc.2010.08.004

[48] Newnham, R.E. (2005) Properties of Materials: Anisotropy, Symmetry, Structure. Oxford University Press.

[49] Gaillac, R., Pullumbi, P. and Coudert, F. (2016) ELATE: An Open-Source Online Application for Analysis and Visualization of Elastic Tensors. *Journal of Physics: Condensed Matter*, **28**, Article 275201. https://doi.org/10.1088/0953-8984/28/27/275201

[50] Wachter, P., Filzmoser, M. and Rebizant, J. (2001) Electronic and Elastic Properties of the Light Actinide Tellurides. *Physica B: Condensed Matter*, **293**, 199-223. https://doi.org/10.1016/s0921-4526(00)00575-5

[51] Sayetat, F., Fertey, P. and Kessler, M. (1998) An Easy Method for the Determination of Debye Temperature from Thermal Expansion Analyses. *Journal of Applied Crystallography*, **31**, 121-127. https://doi.org/10.1107/s0021889897006936

[52] Laramore, G.E. (1972) Energy Dependence of the Effective Debye Temperature Obtained from Low-Energy-Electron-Diffraction-Intensity Measurements. *Physical Review B*, **6**, 1097-1105. https://doi.org/10.1103/physrevb.6.1097

[53] Anderson, O.L. (1963) A Simplified Method for Calculating the Debye Temperature from Elastic Constants. *Journal of Physics and Chemistry of Solids*, **24**, 909-917. https://doi.org/10.1016/0022-3697(63)90067-2

[54] Fine, M.E., Brown, L.D. and Marcus, H.L. (1984) Elastic Constants versus Melting Temperature in Metals. *Scripta Metallurgica*, **18**, 951-956. https://doi.org/10.1016/0036-9748(84)90267-9

[55] Patel, S.B., Srivastava, A., Sharma, R., Abraham, J.A. and Srivastava, V. (2022) Prediction of Structural, Electronic, Mechanical, Thermal, and Thermoelectric Properties in $PbMO_3$ (M=Sb, Bi) Perovskite Compounds: A DFT Study. *The European Physical Journal Plus*, **137**, Article No. 380. https://doi.org/10.1140/epjp/s13360-022-02580-3

[56] König, C., Greer, J.C. and Fahy, S. (2021) Effect of Strain and Many-Body Corrections on the Band Inversions and Topology of Bismuth. *Physical Review B*, **104**, Article 035127. https://doi.org/10.1103/physrevb.104.035127

[57] Sharma, R., Dey, A., Ahmed Dar, S. and Srivastava, V. (2021) A DFT Investigation of $CsMgX_3$ (X=Cl, Br) Halide Perovskites: Electronic, Thermoelectric and Optical Properties. *Computational and Theoretical Chemistry*, **1204**, Article 113415. https://doi.org/10.1016/j.comptc.2021.113415

[58] Driessen, E.F.C. and de Dood, M.J.A. (2009) The Perfect Absorber. *Applied Physics Letters*, **94**, Article 171109. https://doi.org/10.1063/1.3126062

[59] Butt, M.K., Yaseen, M., Ghaffar, A. and Zahid, M. (2020) First Principle Insight into the Structural, Optoelectronic, Half Metallic, and Mechanical Properties of Cubic Perovskite $NdInO_3$. *Arabian Journal for Science and Engineering*, **45**, 4967-4974. https://doi.org/10.1007/s13369-020-04576-6

[60] Ahmed, M.T., Islam, S. and Ahmed, F. (2023) A-Site Cation Replacement of Hydrazinium Lead Iodide Perovskites by Borane Ammonium Ions: A DFT Calculation. *ChemistryOpen*, **13**, e202300207. https://doi.org/10.1002/open.202300207

[61] Levine, Z.H. and Louie, S.G. (1982) New Model Dielectric Function and Exchange-Correlation Potential for Semiconductors and Insulators. *Physical Review B*, **25**, 6310-6316. https://doi.org/10.1103/physrevb.25.6310

[62] Prokopidis, K. and Kalialakis, C. (2014) Physical Interpretation of a Modified Lorentz Dielectric Function for Metals Based on the Lorentz-Dirac Force. *Applied Physics B*, **117**, 25-32. https://doi.org/10.1007/s00340-014-5794-1

[63] Rezaei Niya, S.M. and Hoorfar, M. (2013) Study of Proton Exchange Membrane Fuel Cells Using Electrochemical Impedance Spectroscopy Technique—A Review. *Journal of Power Sources*, **240**, 281-293. https://doi.org/10.1016/j.jpowsour.2013.04.011

[64] Tripathy, S.K. and Kumar, V. (2014) Electronic, Elastic and Optical Properties of $ZnGeP_2$ Semiconductor under Hydrostatic Pressures. *Materials Science and Engineering: B*, **182**, 52-58. https://doi.org/10.1016/j.mseb.2013.11.020

[65] Ephraim Babu, K., Murali, N., Vijaya Babu, K., Taddesse Shibeshi, P. and Veeraiah, V. (2014) Structural, Elastic, Electronic, and Optical Properties of Cubic Perovskite $CsCaCl_3$ Compound: An *ab initio* Study. *Acta Physica Polonica A*, **125**, 1179-1185. https://doi.org/10.12693/aphyspola.125.1179